Modal method in deep metal–dielectric gratings: the decisive role of hidden modes

Maud Foresti and Ludivine Menez

Saint-Gobain Recherche, 39, quai Lucien Lefranc BP135, F-93303 Aubervilliers, France

Alexander V. Tishchenko

Hubert Curien Laboratory, University Jean Monnet, 18 rue Benoit Lauras, Batiment F, F-42000 Saint-Etienne, France

Received February 6, 2006; revised April 14, 2006; accepted April 18, 2006; posted May 17, 2006 (Doc. ID 67735)

The modal method is well adapted for the modeling of deep-groove, high-contrast gratings of short period, possibly involving metal parts. Yet problems remain in the case of the TM polarization in the presence of metal parts in the corrugations: whereas most of the diffraction features are explained by the interplay of an astonishingly small number of true propagating and low-order evanescent modes, the exact solution of the diffraction problem requires the contribution of two types of evanescent modes that are usually overlooked. We investigate the nature and the role of these modes and show that metal gratings can be treated exactly by the modal method. © 2006 Optical Society of America

OCIS codes: 050.1950, 050.1960.

1. INTRODUCTION

The modal method is often applied to one-dimensional (1D) periodic corrugations in its rigorous-coupled-wave-analysis form whereby the permittivity profile $\epsilon(x,z)$ in the grating region is expressed as a Fourier series.[1] The electromagnetic field is also expressed in a Fourier series which can be summed to represent the field of the modes propagating up and down the grooves of the corrugation. These modes are, however, the modes of the Fourier-developed grating profile, not of the actual grating. In the presence of high index contrast, and particularly when metal parts are involved, such approach faces convergence problems.[2]

The true modal method[3] considers the corrugation as it actually is and calculates the field as that of the modes satisfying the boundary conditions at the grating walls. High permittivity contrasts are therefore taken into account naturally, which results in much faster convergence. In a lamellar grating, the propagation constant of the modes is given analytically as the solution of a very simple dispersion equation resulting from the periodic boundary conditions at the groove interfaces.

The presence of metal in the case of the TM polarization is known to cause numerical problems in most methods.[2] The modal method also meets difficulties, although the modes propagating up and down the rectangular grooves of the grating do represent a natural basis for the expansion of the grating fields.[4] The modal method gives correct results if all the modes are taken into account. It is usually believed on the basis of early fundamental work that the modes of a lossless lamellar grating have either real or imaginary eigenvalues.[5] Applying this statement to a lamellar grating comprising lossless metal parts actually leads to wrong results. Indeed, there are some modes exhibiting a complex eigenvalue even in a lossless structure.[6] When they are considered as parts of the modal basis, the modal method gives diffraction efficiencies of a lossy grating with high accuracy and much greater speed than the Fourier modal methods.

2. MODAL METHOD IN PERIODIC STRUCTURES

A. One-Dimensional Binary Grating

Let us consider the diffraction of a plane monochromatic wave on a lamellar grating made in a layer of thickness h between two semi-infinite homogeneous media of permittivity ϵ_{I} and ϵ_{II} (see Fig. 1). The grating contains two types of interleaved bars having thickness d_1, d_2 and permittivity ϵ_{1g}, ϵ_{2g}, respectively, of period $d=d_1+d_2$ in the x direction. The magnetic permeability of all media is assumed to be that of vacuum μ_0. The structure is uniform in the y direction. If the incidence is under angle θ relative to the z axis, the field components of the incident wave are

$$\begin{pmatrix} \mathbf{E}_i(x,z,t) \\ \mathbf{H}_i(x,z,t) \end{pmatrix} = \begin{pmatrix} \mathbf{E}_0^{\mathrm{I}+} \\ \mathbf{H}_0^{\mathrm{I}+} \end{pmatrix} \exp(ik_x x)\exp(-ik_0^{\mathrm{I}} z)\exp(-i\omega t), \tag{1}$$

where

$$k_x = k_0 n_{\mathrm{I}} \sin\theta, \qquad k_0^{\mathrm{I}} = k_0 n_{\mathrm{I}} \cos\theta, \tag{2}$$

$$\epsilon_{\mathrm{I}} = n_{\mathrm{I}}^2 \epsilon_0, \qquad k_0 = \omega\sqrt{\epsilon_0 \mu_0}. \tag{3}$$

The rationale of the modal method is to first represent the field inside the grating in the form of modes of an infinite periodical structure and then to match the grating modes at interfaces $z=\pm h/2$ with diffraction order fields under and above the grating. Thus, the field solution in the grating region is expressed as the infinite sum

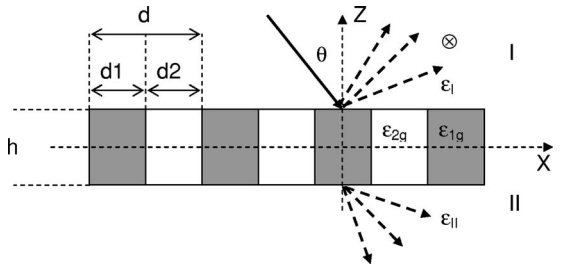

Fig. 1. Plane wave diffraction from a lamellar grating.

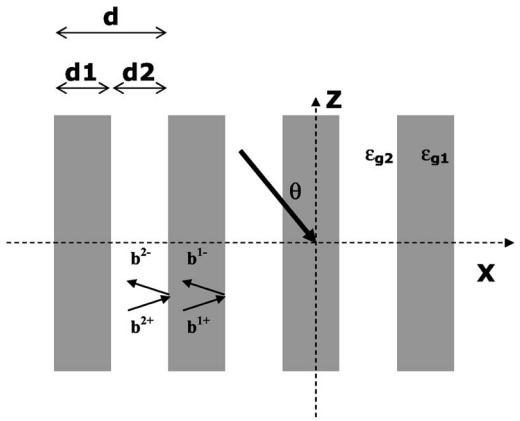

Fig. 2. Modal field representation in an infinite grating.

$$\begin{pmatrix}\mathbf{E}_d(x,z)\\ \mathbf{H}_d(x,z)\end{pmatrix}=\sum_{q=0}^{\infty}\begin{pmatrix}\mathbf{E}_q(x)\\ \mathbf{H}_q(x)\end{pmatrix}[a_q^+\exp(i\beta_q z)+a_q^-\exp(-i\beta_q z)],$$

$$-\frac{h}{2}<z<\frac{h}{2}, \tag{4}$$

where, for the mode of order q, β_q is the propagation constant, $a_q^{\pm}$ are up and down wave amplitudes, and $\begin{pmatrix}\mathbf{E}_q(x)\\ \mathbf{H}_q(x)\end{pmatrix}$ is the quasi-periodical part of the modal field distribution. The following subsections will be devoted to determining the propagation constants β_q and modal fields. The unknown amplitudes $a_q^{\pm}$ can be found by using boundary conditions at interfaces $z=\pm h/2$.

B. Modes of an Infinite Grating

The grating is first considered as infinite in the z direction. Let a grating mode propagate with constant β_q up in the z direction. In both media of which the grating is compared the mode is represented by two waves (Fig. 2). At vertical interfaces these waves are partially reflected and transmitted. Since such reflection/transmission does not change the polarization, each mode of the grating is either TE or TM polarized.

1. TE Grating Modes

The electric field of a TE mode has only a transverse component directed along the y axis. Besides its periodicity, it contains the factor proportional to $\exp(ik_x x)$ imposed by the incident wave. Therefore, over the mth period of the grating the modal field can be found in the form

$$\mathbf{E}_q(x,y,z,t)=\mathbf{n}_y\exp(ik_x md)\exp(i\beta_q z)\exp(-i\omega t)\times\begin{cases}b_q^{1+}\exp(ik_1x)+b_q^{1-}(-ik_1x), & md\leqslant x\leqslant md+d_1\\ b_q^{2+}\exp(ik_2x)+b_q^{2-}\exp(-ik_2x), & md+d_1\leqslant x\leqslant (m+1)d\end{cases}, \tag{5}$$

where

$$k_j=\sqrt{k_0{}^2n_{jg}{}^2-\beta_q{}^2},\quad j=1,2, \tag{6}$$

m is an arbitrary integer number, β_q is the propagation constant, and amplitudes $b_q^{j\pm}$, $j=1,2$, are to be determined.

The continuity of the electric field and of its x derivative at interfaces $x=md$ and $x=md+d_1$ gives the relationships between amplitudes $b_q^{j\pm}$, $j=1,2$, as well as the dispersion equation on the propagation constant β_q:

$$\cos k_1d_1\cos k_2d_2-\frac{1}{2}\left(\frac{k_1}{k_2}+\frac{k_2}{k_1}\right)\sin k_1d_1\sin k_2d_2=\cos k_xd. \tag{7}$$

2. TM Grating Modes

The magnetic field of a TM mode over the mth period of the grating is found as

$$\mathbf{H}_q(x,y,z,t)=\mathbf{n}_y\exp(ik_x md)\exp(i\beta_q z)\exp(-i\omega t)\times\begin{cases}b_q^{1+}\exp(ik_1x)+b_q^{1-}(-ik_1x), & md\leqslant x\leqslant md+d_1\\ b_q^{2+}\exp(ik_2x)+b_q^{2-}\exp(-ik_2x), & md+d_1\leqslant x\leqslant (m+1)d\end{cases}. \tag{8}$$

The continuity of the magnetic field H_y and of ratio $(1/\epsilon)\times(\partial H_y/\partial x)$ at interfaces $x=md$ and $x=md+d_1$ gives the relationships between coefficients $b_q^{j\pm}$, $j=1,2$, as well as the dispersion equation on the propagation constant:

$$\cos k_1d_1\cos k_2d_2-\frac{1}{2}\left(\frac{n_{2g}{}^2k_1}{n_{1g}{}^2k_2}+\frac{n_{1g}{}^2k_2}{n_{2g}{}^2k_1}\right)\sin k_1d_1\sin k_2d_2=\cos k_xd. \tag{9}$$

More detailed derivation of Eqs. (7) and (9) can be found in Refs. 3 and 5–8.

3. DISPERSION EQUATION ANALYSIS

In Sections 3 and 4, the case of a purely real dielectric permittivity is considered. This simplifies substantially the modal analysis without any loss of physical meaning. The case of lossy metals will be analyzed in Section 5.

Both dispersion equations contain the square of propagation constant β_q only. This means that the mode propagates up and down the grating with the same propagation constant. The dispersion equation analysis is reduced to the analysis of dispersion functions $f_{TE}(\rho)$ and $f_{TM}(\rho)$:

$$f_{TE}(\rho) = \cos(k_0 d_1 \sqrt{n_{1g}^2 - \rho})\cos(k_0 d_2 \sqrt{n_{2g}^2 - \rho}) - \frac{1}{2}\left(\frac{\sqrt{n_{1g}^2 - \rho}}{\sqrt{n_{2g}^2 - \rho}} + \frac{\sqrt{n_{2g}^2 - \rho}}{\sqrt{n_{1g}^2 - \rho}}\right) \times \sin(k_0 d_1 \sqrt{n_{1g}^2 - \rho})\sin(k_0 d_2 \sqrt{n_{2g}^2 - \rho}), \quad (10)$$

$$f_{TM}(\rho) = \cos(k_0 d_1 \sqrt{n_{1g}^2 - \rho})\cos(k_0 d_2 \sqrt{n_{2g}^2 - \rho}) - \frac{1}{2}\left(\frac{n_{2g}^2\sqrt{n_{1g}^2 - \rho}}{n_{1g}^2\sqrt{n_{2g}^2 - \rho}} + \frac{n_{1g}^2\sqrt{n_{2g}^2 - \rho}}{n_{2g}^2\sqrt{n_{1g}^2 - \rho}}\right) \times \sin(k_0 d_1 \sqrt{n_{1g}^2 - \rho})\sin(k_0 d_2 \sqrt{n_{2g}^2 - \rho}), \quad (11)$$

where parameter ρ represents the square of the modal effective index:

$$\rho_q = (\beta_q / k_0)^2. \quad (12)$$

The values ρ_q are found as correspondent solutions of the dispersion Eqs. (7) and (9):

$$f(\rho) = \cos k_x d. \quad (13)$$

Since all quantities in the dispersion equation are real, the complex conjugate ρ_q^* of any solution ρ_q will be also a solution of Eq. (13). Thus, all eigenvalues are either real or appear as a pair of complex conjugates.

The left-hand side of the dispersion equation contains only grating parameters and does not depend on the incidence conditions. Therefore, the analysis of function $f(\rho)$ can be performed independently of the incidence. Without loss of generality, let $n_{1g}^2 < n_{2g}^2$.

The analysis of the dispersion equations reveals that there are two substantially different electromagnetic structures. The first type of electromagnetic structure concerns the TE polarization in all types of gratings and the TM polarization in purely dielectric gratings ($n_{1g}^2 > 0$) or purely metallic gratings ($n_{2g}^2 < 0$). A similar behavior in all these gratings is expected since the only difference between functions $f_{TE}(\rho)$ and $f_{TM}(\rho)$ is given by the permittivity ratio; this ratio is always positive and the sign of the second term of the dispersion equation is not changed. For the sake of brevity, this case is referred to here as the *ordinary* case. The second type of electromagnetic structure concerns the TM polarization in a metal–dielectric grating ($n_{1g}^2 < 0, n_{2g}^2 > 0$). The permittivity ratio is now negative and the sign of the second term in the dispersion equation is changed. This type of electromagnetic structure will be referred to as the *special* case.

There are three different domains of solutions for ρ_q with respect to n_{1g}^2 and n_{2g}^2:

1. $\rho > n_{2g}^2$,
2. $n_{1g}^2 < \rho < n_{2g}^2$,
3. $\rho < n_{1g}^2$.

In the first domain, the ordinary case exhibits no solution since $f(\rho) > 1$ in the whole domain. In the special case, we have $f_{TM}(\rho) \xrightarrow[\rho\to\infty]{} -\infty$. If $n_{1g}^2 + n_{2g}^2 < 0$, then the metal–dielectric interface can support a plasmon mode with

$$\rho_{pl} = \frac{n_{1g}^2 n_{2g}^2}{n_{1g}^2 + n_{2g}^2}. \quad (14)$$

It can be shown that $\rho_{pl} > n_{2g}^2$, $f(\rho_{pl}) > 1$, and the existence of a modal solution in the domain $\rho > \rho_{pl}$ follows from the continuity of $f(\rho)$. Such mode is similar to a short-range plasmon mode on a single thin metal layer.[9] Evidently, it cannot have any analog in the ordinary case.

It is well known that a thin metal layer can support a long-range plasmon as well.[10] The corresponding grating mode exists when $f(n_{2g}^2) < 0$, so the distance between two neighboring metal sheets has to be large enough.

In the second domain, the solutions of Eq. (13) are modes of the second (dielectric in the special case) layer. No specific difference exists in the domain considered between ordinary and special cases.

The main difference between two cases is found in the third domain, $\rho < \epsilon_{1g}$. First, consider the ordinary case. Function $f_{TE}(\rho)$ can be rewritten in the form

$$f_{TE}(\rho) = \frac{1}{4}\left(\sqrt{\frac{\sqrt{n_{1g}^2 - \rho}}{\sqrt{n_{2g}^2 - \rho}}} + \sqrt{\frac{\sqrt{n_{2g}^2 - \rho}}{\sqrt{n_{1g}^2 - \rho}}}\right)^2 \times \cos(k_0 d_1 \sqrt{n_{1g}^2 - \rho} + k_0 d_2 \sqrt{n_{2g}^2 - \rho}) - \frac{1}{4}\left(\sqrt{\frac{\sqrt{n_{1g}^2 - \rho}}{\sqrt{n_{2g}^2 - \rho}}} - \sqrt{\frac{\sqrt{n_{2g}^2 - \rho}}{\sqrt{n_{1g}^2 - \rho}}}\right)^2 \times \cos(k_0 d_1 \sqrt{n_{1g}^2 - \rho} - k_0 d_2 \sqrt{n_{2g}^2 - \rho}). \quad (15)$$

Any solution ρ_m of the equation

$$k_0 d_1 \sqrt{n_{1g}^2 - \rho} + k_0 d_2 \sqrt{n_{2g}^2 - \rho} = m\pi \quad (16)$$

satisfies the condition $|f_{TE}(\rho_m)| \geq 1$, since

$$\frac{1}{4}\left(\sqrt{\frac{\sqrt{n_{1g}^2 - \rho}}{\sqrt{n_{2g}^2 - \rho}}} + \sqrt{\frac{\sqrt{n_{2g}^2 - \rho}}{\sqrt{n_{1g}^2 - \rho}}}\right)^2 = \frac{1}{4}\left(\sqrt{\frac{\sqrt{n_{1g}^2 - \rho}}{\sqrt{n_{2g}^2 - \rho}}} - \sqrt{\frac{\sqrt{n_{2g}^2 - \rho}}{\sqrt{n_{1g}^2 - \rho}}}\right)^2 + 1. \quad (17)$$

Note, that odd m results in negative values of $f_{TE}(\rho_m)$ whereas even m gives positive values of $f_{TE}(\rho_m)$. Hence, every mode can be found between two consecutive points ρ_m [except for the case $|f_{TE}(\rho_m)| = 1$, when two modes are

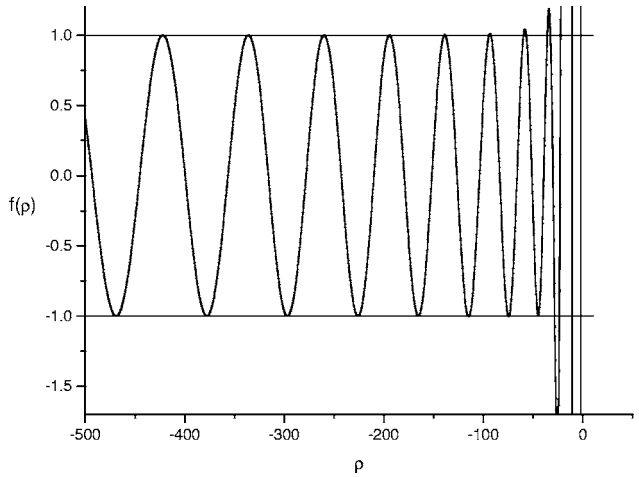

Fig. 3. TE dispersion curve in a metal–dielectric grating.

degenerated]. The numerical example in Fig. 3 illustrates a typical behavior of function $f(\rho)$ in the ordinary case (metal–dielectric grating and TE polarization). The grating period is 200 nm with 0.5 line/period ratio. Grating layers are Al and air ($n_{1g}^2=-25$, $n_{2g}^2=1$), the wavelength is 450 nm.

An approximate modal location is determined by condition (16). The number of modes at a given value of ρ corresponds to the whole "optical thickness" of one grating period $k_1d_1+k_2d_2$. In this context, each grating mode belongs to the whole structure. In the limit of high mode order, when $k_1 \cong k_2 \cong \sqrt{-\rho}$, the density of grating modes depends only on the ratio d/λ. This remains true in the presence of the permittivity ratios in the function $f_{\mathrm{TM}}(\rho)$ for the TM mode in the ordinary case.

However, the behavior of the modal solutions is quite different in the special case. In this case, function $f_{\mathrm{TM}}(\rho)$ is written as

$$f_{\mathrm{TM}}(\rho) = \frac{1}{4}\left(\sqrt{\frac{n_{2g}^2\sqrt{n_{1g}^2-\rho}}{|n_{1g}^2|\sqrt{n_{2g}^2-\rho}}} + \sqrt{\frac{|n_{1g}^2|\sqrt{n_{2g}^2-\rho}}{n_{2g}^2\sqrt{n_{1g}^2-\rho}}} \right)^2 \times \cos(k_0 d_1 \sqrt{n_{1g}^2-\rho} - k_0 d_2 \sqrt{n_{2g}^2-\rho}) - \frac{1}{4}\left(\sqrt{\frac{n_{2g}^2\sqrt{n_{1g}^2-\rho}}{|n_{1g}^2|\sqrt{n_{2g}^2-\rho}}} - \sqrt{\frac{|n_{1g}^2|\sqrt{n_{2g}^2-\rho}}{n_{2g}^2\sqrt{n_{1g}^2-\rho}}} \right)^2 \times \cos(k_0 d_1 \sqrt{n_{1g}^2-\rho} + k_0 d_2 \sqrt{n_{2g}^2-\rho}). \quad (18)$$

Similar to the previous analysis one concludes that at least one modal solution is found between two consecutive solutions of the equation

$$k_0 d_1 \sqrt{n_{1g}^2-\rho} - k_0 d_2 \sqrt{n_{2g}^2-\rho} = m\pi. \quad (19)$$

The density of such solutions is less than that given by Eq. (16). The numerical example of Fig. 4 confirms this statement. The high frequency term $k_1d_1+k_2d_2$ generates modal solutions for each intersection of curve $f_{\mathrm{TM}}(\rho)$ with horizontal line $\cos(k_xd)$. The difference in the ordinary case is that the lower-frequency term in Eq. (19) has much larger amplitude than the high-frequency term. This leads to the possible separation of curve $f_{\mathrm{TM}}(\rho)$ and line $\cos(k_xd)$. When, for instance, a local maximum of $f_{\mathrm{TM}}(\rho)$ is under line $\cos(k_xd)$, there is no longer any intersection. At first glance, it would seem that no mode exists in this domain. But this is not true. It was mentioned in Ref. 6 that, similar to algebraic second-order polynomials, in the absence of real roots two complex conjugate solutions exist in the vicinity of each such extremum of $f_{\mathrm{TM}}(\rho)$. Mathematical evidence of such solutions requires, however, a physical interpretation. This is very important for four reasons. First, the existence of such solutions, even though they were mentioned in Ref. 6, was then ignored,[11] and even denied[5,12] by other authors, who claimed that any grating with purely real permittivities possesses only modes with purely real values ρ_m. This claim is misleading and needs to be countered. Second, the analysis of such complex ("hidden") modes reveals interesting physical analogies. Third, these modes complete the modal basis to the modal density given by Eq. (16). Finally, "hidden" modes must be taken into account in any implementation of the modal method for solving diffraction problems exactly.

Table 1 represents the results of a numerical example in which the diffraction efficiency is calculated both accounting for and neglecting the hidden modes. The lamellar grating of period 200 nm with 0.5 line/period ratio is made in an Al layer of 521 nm thickness ($n_{1g}^2=-25, n_{2g}^2=1$) on a glass substrate ($n_{\mathrm{II}}^2=2.25$), the wavelength is 450 nm, the angle of incidence is 35° from the air side ($n_{\mathrm{I}}^2=1$), the polarization is TM (the special case). From Table 1 it is clear that increasing the number of evanescent modes and evanescent diffraction orders considered does not improve the convergence if the hidden modes are neglected. Obviously, the role of hidden modes is crucial in this example.

The present analysis is not sufficient when the line/space ratio of the grating is very small and/or very large. Consider, for example, the case $d_1 \gg d_2$. Two frequencies in formula (18) are not very different and this perturbs the solution behavior. The modal location is no longer determined by Eq. (16). A more appropriate expression of function $f_{\mathrm{TM}}(\rho)$ is

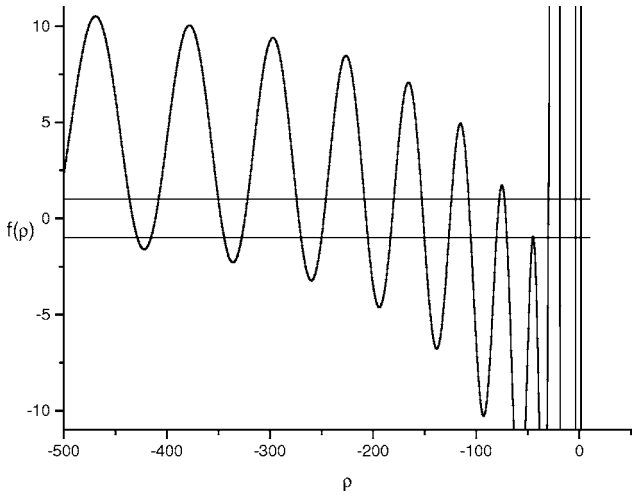

Fig. 4. TM dispersion curve; the grating and the incident wave are the same as in Fig. 3.

Table 1. Zeroth-Order TM Diffraction on a Lossless Metal–Dielectric Grating, $d_1/d=0.5$

Number of Modes	Complete Modal Basis		Neglecting Hidden Modes	
	Transmission	Reflection	Transmission	Reflection
5	0.8901921475	0.1016072281	0.8901921475	0.1016072281
9	0.8765922481	0.1114728698	1.0389528710	0.1796275371
17	0.8751616505	0.1212803594	1.1484419400	0.2485328513
33	0.8735083902	0.1254448768	0.8529418663	0.3579954386
65	0.8727351564	0.1269459890	0.9426439135	0.1232907240
129	0.8724474463	0.1274520496	0.7062587589	0.0430437874
257	0.8723493545	0.1276183215	0.2521742909	0.6473278467
513	0.8723171226	0.1276723836	0.9229722058	0.1901889377
1025	0.8723067032	0.1276898787	0.7972451570	0.0396516471

$$f_{\mathrm{TM}}(\rho)=\sqrt{1+\frac{1}{4}\left(\frac{n_{2g}^{2}\sqrt{n_{1g}^{2}-\rho}}{|n_{1g}^{2}|\sqrt{n_{2g}^{2}-\rho}}-\frac{|n_{1g}^{2}|\sqrt{n_{2g}^{2}-\rho}}{n_{2g}^{2}\sqrt{n_{1g}^{2}-\rho}}\right)^{2}\sin^{2}(k_0d_1\sqrt{n_{1g}^{2}-\rho})}\times\cos\left\{k_0d_2\sqrt{n_{2g}^{2}-\rho}+\arctan\left[\frac{1}{2}\left(\frac{n_{2g}^{2}\sqrt{n_{1g}^{2}-\rho}}{|n_{1g}^{2}|\sqrt{n_{2g}^{2}-\rho}}+\frac{|n_{1g}^{2}|\sqrt{n_{2g}^{2}-\rho}}{n_{2g}^{2}\sqrt{n_{1g}^{2}-\rho}}\right)\tan(k_0d_1\sqrt{n_{1g}^{2}-\rho})\right]\right\}. \tag{20}$$

A typical behavior of $f_{\mathrm{TM}}(\rho)$ is shown in Fig. 5. Evidently, each intersection of curve $f_{\mathrm{TM}}(\rho)$ with line $\cos(k_xd)$ gives a mode. Since the amplitude factor in Eq. (18) is at least unity, one mode is found between two consecutive solutions of the equation

$$k_0d_2\sqrt{n_{2g}^{2}-\rho}-\arctan\left[\frac{1}{2}\left(\frac{n_{2g}^{2}\sqrt{n_{1g}^{2}-\rho}}{|n_{1g}^{2}|\sqrt{n_{2g}^{2}-\rho}}+\frac{|n_{1g}^{2}|\sqrt{n_{2g}^{2}-\rho}}{n_{2g}^{2}\sqrt{n_{1g}^{2}-\rho}}\right)\tan(k_0d_1\sqrt{n_{1g}^{2}-\rho})\right]=m\pi. \tag{21}$$

The analysis reveals that the density of modes given by Eq. (21) is the same as defined by Eq. (19), and it is not sufficient for completing the modal basis. Some modes are missing. In order to localize them, let us consider the case $k_1d_1\cong m\pi$. Then, Eq. (21) becomes

$$1+\frac{1}{8}\left(\frac{n_{2g}^{2}\sqrt{n_{1g}^{2}-\rho}}{|n_{1g}^{2}|\sqrt{n_{2g}^{2}-\rho}}-\frac{|n_{1g}^{2}|\sqrt{n_{2g}^{2}-\rho}}{n_{2g}^{2}\sqrt{n_{1g}^{2}-\rho}}\right)^{2}(k_0d_1\sqrt{n_{1g}^{2}-\rho}-m\pi)^{2}\cong\frac{\cos(k_xd)}{\cos(k_0d_2\sqrt{n_{2g}^{2}-\rho})}, \tag{22}$$

from which we get two complex roots:

$$k_1d_1\cong m\pi\pm j\sqrt{8}\frac{\sqrt{1-\dfrac{\cos(k_xd)}{\cos(k_0d_2\sqrt{n_{2g}^{2}-\rho})}}}{\left|\dfrac{n_{2g}^{2}\sqrt{n_{1g}^{2}-\rho}}{|n_{1g}^{2}|\sqrt{n_{2g}^{2}-\rho}}-\dfrac{|n_{1g}^{2}|\sqrt{n_{2g}^{2}-\rho}}{n_{2g}^{2}\sqrt{n_{1g}^{2}-\rho}}\right|}. \tag{23}$$

Such roots correspond to hidden modes of a new type. They have never been mentioned before in the literature. Similar to the hidden modes of the first type, they are very important in diffraction analysis. This fact is illustrated in Table 2 where all the structure parameters are

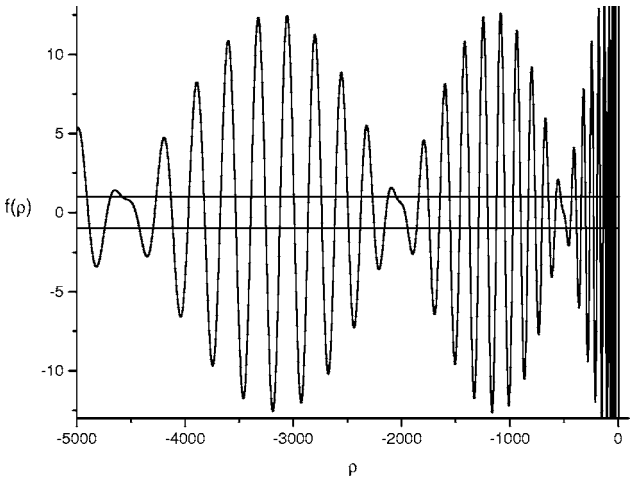

Fig. 5. TM dispersion curve in a case of metal–dielectric grating with line/period ratio of 0.95. All other parameters are the same as in Fig. 3.

Table 2. Zeroth-Order TM Diffraction on a Lossless Metal–Dielectric Grating, $d_1/d=0.95$

Number of Modes	Complete Modal Basis		Neglecting Hidden Modes	
	Transmission	Reflection	Transmission	Reflection
15	0.6572419397	0.3376533362	0.6572419397	0.3376533362
20	0.7674317175	0.2770071826	0.7248961953	0.2345484121
30	0.8048567964	0.195968401	0.7898380007	0.1902391117
50	0.792087328	0.2083842497	0.6882089302	0.1467750505
90	0.8002786777	0.199947763	0.6082492786	0.2125015272
170	0.8028587367	0.1972342546	0.3448335686	0.3976552843
330	0.8036283887	0.1964062279	0.1759741614	0.5597773657
650	0.8038538188	0.1961583539	0.2360555576	0.1168753608
1290	0.8039192353	0.1960849089	0.323986926	0.07356533296

taken the same as in the previous example of Table 1, but the line/space ratio of the grating is 0.95. The calculated diffraction efficiencies accounting for and neglecting the hidden modes of the second type are presented. The density of such modes is defined by twice the optical thickness of the first layer $k_1 d_1$. Thus, the total modal spectrum in the grating considered can be represented by real modes and hidden modes of the second type.

A quite similar description can be obtained also in the case $d_1 \gg d_2$.

4. NATURE OF HIDDEN MODES

Section 3 explains the important difference between the ordinary and the special cases in the domain $\rho < {n_{1g}}^2$. The two types of hidden modes identified in the special case are the subject of this section.

The first step is to analyze the behavior of the modal fields corresponding to ρ_q in the modal basis. Let us start by considering the ordinary case with the structure parameters those of Fig. 3. The modal fields $\Psi_q(x)=E_y(x)$ represented in Fig. 6 demonstrate that the power in each TE mode is essentially evenly distributed in both layers of the grating. This confirms our conjecture that each mode in the ordinary case pertains to the whole grating period.

Quite different is the situation in the special case. Figure 7 represents the TM modal fields of the grating having the parameters of Fig. 3. Ratio $\Psi_q(x)=H_y(x)/n(x)$ is used rather than field $H_y(x)$ in order to demonstrate the mode power distribution over the grating period. One can conclude that all normal (not hidden) modes of this structure can be assigned two sets: the "dielectric" modes whose power is essentially concentrated in the dielectric layer, and the "metal" modes whose power is mainly in the metal layer.

The power of a hidden mode is evenly divided between the two layers of a period. Considering the fields of two conjugated hidden modes $\Psi_q(x)$ and $\Psi_p(x)$ reveals that in one layer their fields coincide whereas in the other layer they are opposite in phase (see Fig. 8). Therefore, combination $\Psi_q(x)+\Psi_p(x)$ gives rise to a dielectric mode, and combination $\Psi_q(x)-\Psi_p(x)$ to a metal one. Such modal behavior is well known in the coupled-mode theory[13]: When two neighboring modes are coupled, the eigenmode field is represented by a combination of the coupled modal fields. Thus, the described field behavior allows the hypothesis

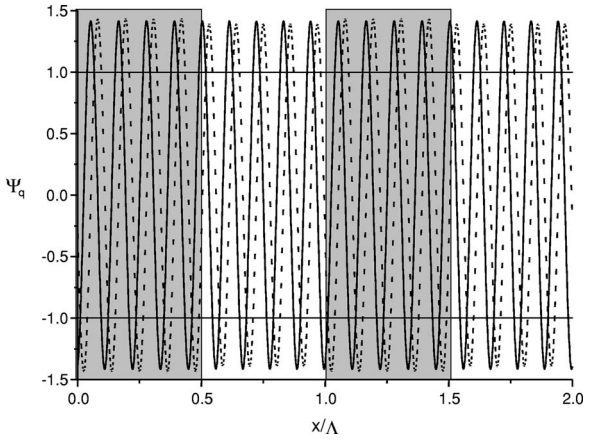

Fig. 6. TE mode field distribution, modes $m=17$ (solid curve) and $m=18$ (dashed curve). The modal fields are evenly distributed over the whole period of the grating.

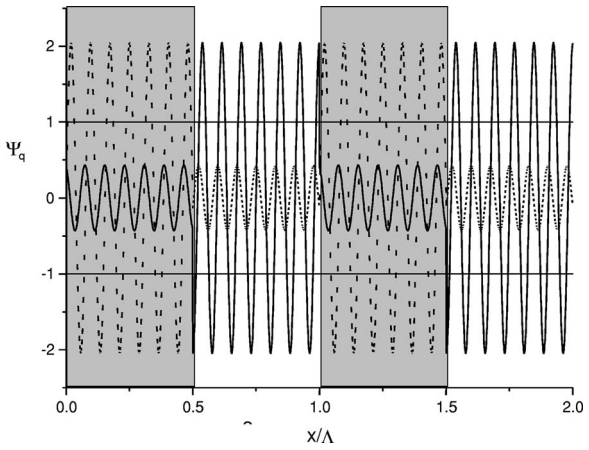

Fig. 7. TM mode field distribution, mode $m=25$; solid curve—the power is located mostly in the dielectric layer—and $m=26$; dashed curve—the power is located mostly in the metal layer.

that a pair of hidden modes of a grating is the result of the coupling between a dielectric and a metal mode.

A similar behavior of the modal fields is found in the case of a small line/space ratio. Figure 9 represents the modal fields of the grating structure with very narrow slits having the same parameters as in Fig. 5. One can conclude that all nonhidden modes of this structure are

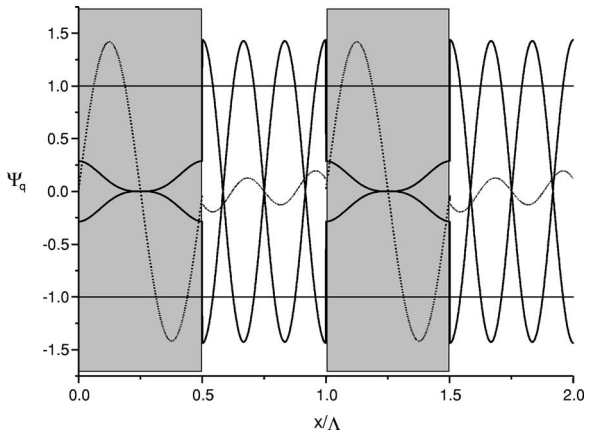

Fig. 8. Pair of hidden modes, $m=4$ and $m=5$. The real parts of modal fields coincide (dashed curve), whereas the imaginary parts are in phase opposition (solid curve). Two grating periods are represented; the metal parts are shaded.

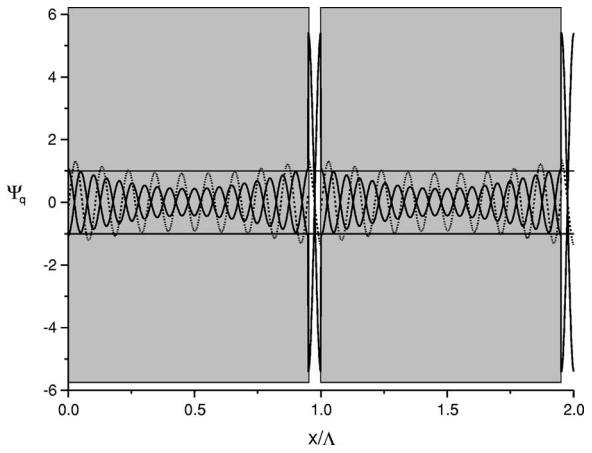

Fig. 9. Pair of hidden modes, $m=19$ and $m=20$. The real parts of modal fields coincide (dashed curve), whereas the imaginary parts are in phase opposition (solid curve). Two grating periods are represented; the metal parts are shaded.

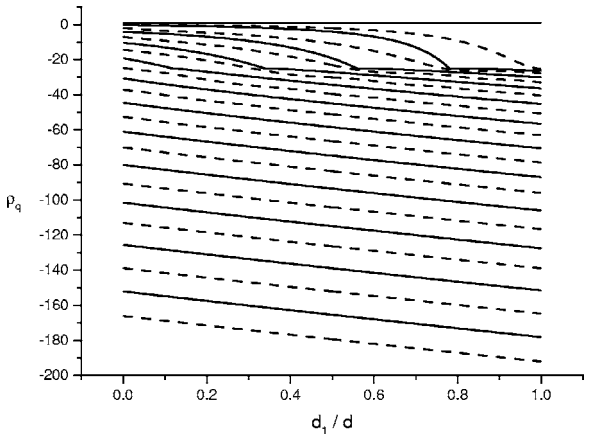

Fig. 10. Diagram representing the square of propagation constants ρ_q of TE modes versus the line/period ratio d_1/d (ordinary case). The dispersion curves (dashed) are well separated and lie between the characteristic curves determined by condition (16) (solid curves). The grating and the incident wave are the same as in Fig. 3.

modes of the larger (metal) layer whereas each hidden mode is possibly the result of the coupling between a dielectric mode and a metal mode.

Thus, the analysis of the modal field reveals the following difference between the ordinary and the special cases: whereas in the ordinary case all modes are modes of the whole period of the grating, in the special case each nonhidden mode is either a mode of the dielectric layer or a mode of the metal layer; hidden modes are likely to be the result of the coupling between a dielectric and a metal mode. Consequently, the modal constants in the ordinary case are determined approximately by Eq. (16), whereas in the special case the dielectric-mode propagation constants are approximately determined by

$$k_0 d_1 \sqrt{n_{1g}^{\ 2} - \rho} = \pi m_1 \tag{24}$$

and the metal-mode propagation constants by

$$k_0 d_2 \sqrt{n_{2g}^{\ 2} - \rho} = \pi m_2. \tag{25}$$

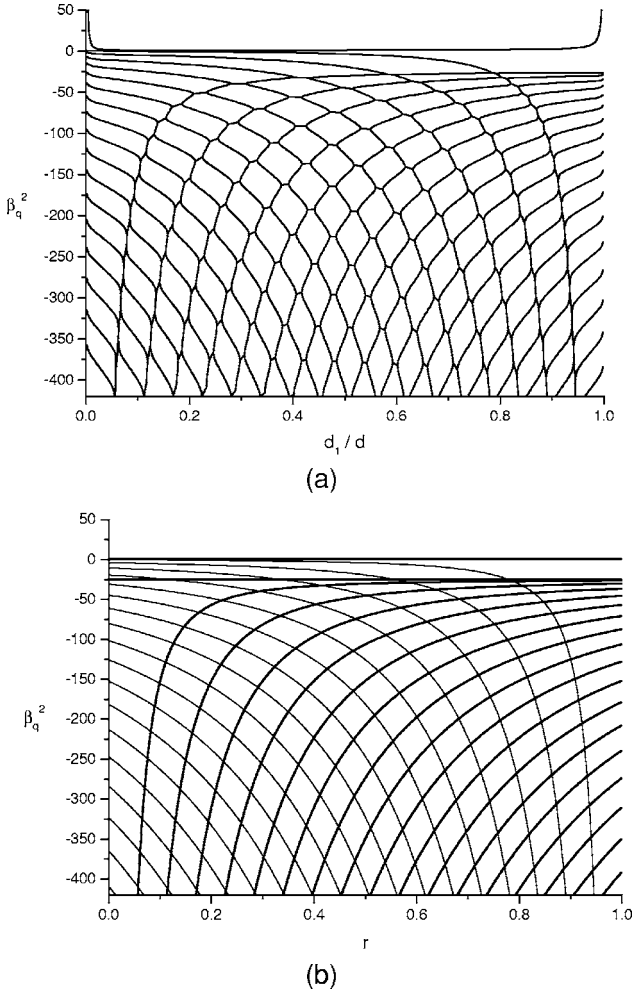

Fig. 11. (a) Diagram representing the real part of ρ_q of TM mode versus the line/period ratio d_1/d (the ordinary case). The dispersion curves can be shown by two sets of curves corresponding to metal-layer modes and to dielectric-layer modes. At the intersection points the modes become coupled with complex ρ_q (hidden modes). (b) Dispersion curves determined by Eqs. (24) and (25) give the location of metal-layer modes (thick curves) and dielectric-layer modes (thin curves).

Table 3. Square Propagation Constants, TE Modes, $d_1/d=0.5$

Order	$\mathrm{Im}(n_{1g}^2)=0$		$\mathrm{Im}(n_{1g}^2)=5$	
q	$\mathrm{Re}(\rho_q)$	$\mathrm{Im}(\rho_q)$	$\mathrm{Re}(\rho_q)$	$\mathrm{Im}(\rho_q)$
0	−2.05773475836	0	−2.07295920390	0.13326506533
1	−10.8291768090	0	−10.9064861515	0.61670054603
2	−23.1000296642	0	−23.45425222803	2.13547169245
3	−30.1348947056	0	−29.94214926509	3.93920329606
4	−39.5715449208	0	−39.57503217304	3.15364964561
5	−51.1365460378	0	−51.08525580678	2.85889571816
6	−66.4798462037	0	−66.44672380113	2.84953454017
7	−83.5735264682	0	−83.55697338848	2.70071372434
8	−101.124242863	0	−104.1029159990	2.69305148615

Table 4. Square Propagation Constants, TM Modes, $d_1/d=0.5$

Order	$\mathrm{Im}(n_{1g}^2)=0$		$\mathrm{Im}(n_{1g}^2)=5$	
q	$\mathrm{Re}(\rho_q)$	$\mathrm{Im}(\rho_q)$	$\mathrm{Re}(\rho_q)$	$\mathrm{Im}(\rho_q)$
0	−1.308478221654	0	1.303053328621	0.03321199859
1	−3.51542358394	0	−3.52306722545	0.04662007691
2	−18.9664152031	0	−18.9369322171	−0.0467210468
3	−30.0581582797	0	−30.0771342070	5.05485675020
4	−44.8471143549	−1.78099134151	−44.3669002919	−0.66478360791
5	−44.8471143549	1.78099134151	−45.3146941451	5.615201278239
6	−71.2738706045	0	−71.1177592973039	5.359179449803
7	−79.3153144201	0	−79.4468585835969	−0.43594054033
8	−106.272295666	0	−106.302125881223	5.268085003609

Table 5. Square Propagation Constants, TM Modes, $d_1/d=0.95$

Order	$\mathrm{Im}(n_{1g}^2)=0$		$\mathrm{Im}(n_{1g}^2)=5$	
q	$\mathrm{Re}(\rho_q)$	$\mathrm{Im}(\rho_q)$	$\mathrm{Re}(\rho_q)$	$\mathrm{Im}(\rho_q)$
0	4.10673104987	0	4.04021871457	0.36291936209
1	−26.3852303210	0	−26.3872352387	5.00675107626
2	−30.5469751851	0	−30.5534775673	5.02327930677
3	−37.5226677947	0	−37.5319362101	5.03537770893
4	−47.2978599407	0	−47.3094083623	5.04709367058
5	−59.9275000913	0	−59.9379856586	5.04454429622
6	−75.3462335770	0	−75.3566621646	5.04599024092
19	−505.7835047673	−21.8341110442	−499.686145533	−22.3885781040
20	−505.7835047673	21.8341110442	−516.514145631	21.29451747704

Note that total modal density $m=m_1+m_2$ will be the same as in the ordinary case.

In order to check these statements the diagram representing ρ_q versus the line/period ratio $r=d_1/d$ is calculated. In the ordinary case (see Fig. 10), the dispersion curves are well separated and lie between the characteristic curves determined by condition (16).

In the special case [see Fig. 11(a)] the dispersion curves are well determined by Eqs. (24) and (25) [Fig. 11(b)]. At the points where two curves of different sets intersect, the dispersion curves are split and the modes become hidden modes with complex value of ρ_q. This confirms our hypothesis that the coupling between modes of different layers is at the origin of a hidden mode.

5. COMPLEX METAL PERMITTIVITY

Although a lossless metal was considered in the previous analysis for the purpose of clarifying the nature of the hidden modes, problems involving lossy metals are treated straightforwardly without additional difficulty.

Considering the previous examples, a lossy metal is now assumed $n_{1g}^2=-25+i5$. One can expect that only

modes whose electric field penetrates deeply into the metal part of the grating will be affected by the change of n_{1g}^2. Table 3 presents solutions of Eq. (7) for the lossless as well as for the lossy metal. Clearly, square effective indices ρ_q acquire an imaginary part that is of the order of $\frac{1}{2}\,\mathrm{Im}(n_{1g}^2)$. This confirms the statement that all the TE evanescent-mode fields belong to the whole period of the grating.

Tables 4 and 5 present solutions ρ_q of Eq. (9) for different line/space ratios. Evidently, all square effective indices of the metal-layer modes acquire an imaginary part that is approximately $\mathrm{Im}(n_{1g}^2)$, whereas the square effective indices of dielectric-layer modes are only slightly changed. Since each hidden mode represents a pair of coupled modes of different kind, their propagation constants' behavior is more complicated.

6. CONCLUSION

The few evanescent TM modes of a metallic grating exhibiting a coupled-mode character even in presence of a lossless metal have been identified and shown to play a decisive role in the general correctness of the original modal method. Once the modes are taken into account, the solution to high index contrast and metallic grating problems is obtained with high accuracy with a small number of modes in a very short time.

All evanescent TM modes of a lamellar grating can be separated into three sets: dielectric-layer modes, metal-layer modes, and coupled dielectric–metal modes. This fact eases considerably the procedure of the root search and can be generalized to any lamellar grating.

ACKNOWLEDGMENTS

The authors thank Gérard Granet for the grating structure example and Nikolai Lyndin for his help in the calculations and fruitful discussions. Olivier Parriaux is gratefully acknowledged for the interest he placed in this work and for contributing to its scope and perspectives. This work was partly carried out in the framework of the European Network of Excellence on Microoptics (NEMO).

A. V. Tishchenko's e-mail address is tishchen @univ-st-etienne.fr.

REFERENCES

1. P. Lalanne and J.-P. Hugonin, "Numerical performance of finite-difference modal methods for the electromagnetic analysis of one-dimensional lamellar gratings," J. Opt. Soc. Am. A **17**, 1033–1042 (2000).
2. T. Vallius, "Comparing the Fourier modal method with the C method: analysis of conducting multilevel gratings in TM polarization," J. Opt. Soc. Am. A **19**, 1555–1562 (2002).
3. L. C. Botten, M. S. Craig, R. C. McPhedran, J. L. Adams, and J. R. Andrewartha, "The dielectric lamellar diffraction grating," Opt. Acta **28**, 413–428 (1981).
4. A. V. Tishchenko, "Phenomenological representation of deep and high contrast lamellar gratings by means of the modal method," Opt. Quantum Electron. **37**, 309–330 (2005).
5. J. Y. Suratteau, M. Cadilhac, and R. Petit, "Sur la détermination numérique des efficacités de certains réseaux diélectriques profonds," J. Opt. (Paris) **14**, 273–288 (1983).
6. P. Sheng, R. S. Stepleman, and P. N. Sanda, "Exact eigenfunctions for square-wave gratings: Application to diffraction and surface-plasmon calculations," Phys. Rev. B **26**, 2907–2916 (1982).
7. R. E. Collin, "Reflection and transmission at a slotted dielectric interface," Can. J. Phys. **34**, 398–411 (1956).
8. S. M. Rytov, "Electromagnetic properties of a finely stratified medium," Sov. Phys. JETP **2**, 466–475 (1956).
9. A. D. Boardman, ed., *Electromagnetic Surface Modes* (Wiley, 1982).
10. D. Sarid, "Long-range surface-plasma waves on very thin metal films," Phys. Rev. Lett. **47**, 1927–1930 (1981).
11. L. C. Botten, M. S. Craig, R. C. McPhedran, J. L. Adams, and J. R. Andrewartha, "The finitely conducting lamellar diffraction grating," Opt. Acta **28**, 1087–1102 (1981).
12. G. Tayeb and R. Petit, "On the numerical study of deep conducting lamellar diffraction gratings," Opt. Acta **31**, 1361–1365 (1984).
13. See, for example, A. Yariv, "Coupled-mode theory for guided-wave optics," IEEE J. Quantum Electron. **9**, 919–933 (1973).